

UNCLASSIFIED



AD NUMBER

AD-041 678

NEW LIMITATION CHANGE

TO

DISTRIBUTION STATEMENT - A

Approved for Public Release; Distribution Unlimited.

LIMITATION CODE: 1

FROM

No Prior DoD Dist'r Scty Statement Assigned.

AUTHORITY

BRL, D/A ltr., dtd April 22, 1981.

THIS PAGE IS UNCLASSIFIED

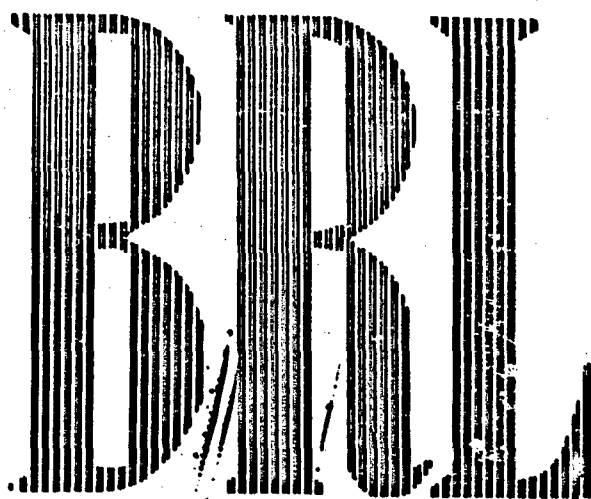
THIS REPORT HAS BEEN DELIMITED  
AND CLEARED FOR PUBLIC RELEASE  
UNDER DOD DIRECTIVE 5200.20 AND  
NO RESTRICTIONS ARE IMPOSED UPON  
ITS USE AND DISCLOSURE.

**DISTRIBUTION STATEMENT A**

APPROVED FOR PUBLIC RELEASE;  
DISTRIBUTION UNLIMITED.

AD No. 41628

ASTIA FILE COPY



REPORT No. 908

**Dynamic Measurements On  
The 81MM Shell T-28E6  
In The National Bureau  
Of Standards Wind Tunnel**

**R. S. MOTT**

DEPARTMENT OF THE ARMY PROJECT No. 503-05-005  
ORDNANCE RESEARCH AND DEVELOPMENT PROJECT No. TB3-0230

**BALLISTIC RESEARCH LABORATORIES**



**ABERDEEN PROVING GROUND, MARYLAND**

**BALLISTIC RESEARCH LABORATORIES**

**REPORT NO. 908**

**MAY 1954**

**DYNAMIC MEASUREMENTS ON THE 81MM SHELL T-2826  
IN THE NATIONAL BUREAU OF STANDARDS WIND TUNNEL**

**R. S. Mott**

**Department of the Army Project No. 503-05-005  
Ordnance Research and Development Project No. TB3-0230**

**ABERDEEN PROVING GROUND, MARYLAND**

## TABLE OF CONTENTS

ABSTRACT . . . . .	5
LIST OF ILLUSTRATIONS . . . . .	3
INTRODUCTION . . . . .	7
I. AXIAL TORQUES	
A. INSTRUMENTATION AND DATA REDUCTION . . . . .	7
B. RESULTS . . . . .	15
II. MAGNUS TORQUE	
A. INSTRUMENTATION AND DATA REDUCTION . . . . .	19
B. RESULTS . . . . .	24
CONCLUSION . . . . .	38

# LIST OF ILLUSTRATIONS

Fig. 1. The BRL - NBS Rig for the Generation of Circular Yawing Motion.	8
Fig. 2. Shell Model Detail.	9
Fig. 3. Fin Types used in Tests.	11
Fig. 4. Representative Plot of Axial Torque vs Spin Function.	13
Fig. 5. Intercepts and Slopes as Functions of Yaw.	17
Fig. 6. Aerodynamic Coefficients of Axial Torque.	18
Fig. 7. Schematic of the BRL - NBS Magnus Torque Balance.	21
Fig. 8. Balance Beam Detail.	23
Fig. 9. Sample Plot of Magnus Torque Data.	27
Fig. 10. Magnus Torque vs Spin and Yaw for T-28 Shell, Standard Fin.	29
Fig. 11. Magnus Torque vs Spin and Yaw for T-28 Shell, Shroudless Standard Fin.	31
Fig. 12. Magnus Torque vs Spin and Yaw for T-28 Shell, Long Fin.	33
Fig. 13. Magnus Torque vs Spin and Yaw for T-28 Shell, Finless.	35
Fig. 14. Comparative Plots of Magnus Torque vs Spin for Various Configurations.	37

BALLISTIC RESEARCH LABORATORIES

REPORT NO. 908

RSMott/lr  
Aberdeen Proving Ground, Md.  
May 1954

DYNAMIC MEASUREMENTS ON THE 81MM SHELL T-28E6  
IN THE NATIONAL BUREAU OF STANDARDS WIND TUNNEL

ABSTRACT

Measurements of the Magnus and axial torques on the 81mm T-28 mortar shell with several fin variants have been performed in the ERL - NBS dynamic measurements rig. The non-linear characteristics of the Magnus and axial torques as noted from the earlier M-56 tests are again evident, and our interpretation of the contributions of the fins and shroud to these torques is corroborated and extended.

## INTRODUCTION

In view of the unexpected non-linearities of Magnus torque found from the tests made on the 81mm M-56 mortar shell, as described in BRL 882\*, the question arose as to whether these characteristics were peculiar to the M-56 shell or were representative of mortar shell in general. The thought was that the M-56 was of poor aerodynamic design, especially in the abrupt step from cylinder to cone that forms a sharp shoulder in the afterbody; and that therefore it was possible that its characteristics were due largely to separation effects which would not be important in the case of shell with a good afterbody shape. Accordingly, another series of dynamic measurements was made, this time on the streamlined 81mm T-28 mortar shell. To determine the effects of the fin, shroud, and increased fin area on the axial and Magnus torques, runs were also made on the T-28 body alone (including tail boom), with a standard fin from which the shroud was removed, and with a long, high-area fin of a design suggested by B. G. Karpov.

These tests were carried out in the summer and fall of 1952 at the National Bureau of Standards' North Wind Tunnel. So as not to delay the measurements and to make them on a comparable basis with the M-56 measurements, the Bureau obligingly postponed its reconstruction of the tunnel working section until the completion of our tests. This paper is a report on these tests.

## I. AXIAL TORQUES

### A. Instrumentation and Data Reduction

The rig for imparting circular yawing motion to the shell model is illustrated in Fig. 1. The shell is mounted on a longitudinal shaft, free to rotate about this shaft on ball bearings. The shaft ends are connected to the supporting wires by means of the nosepiece and ball joint assembly (shown in Fig. 2) which is a low-friction ball-in-cage type of coupling, allowing the shaft to execute circular yawing motion freely without imparting bending stresses to the wires or allowing the shaft itself to rotate. On the outside of the shell, about the center of yawing motion, the circumference is marked with 25 equidistant divisions so that a record of the angular displacement,  $\theta$ , vs time may be made by a motion picture camera. The camera is a 16mm type, running at 30 frames/sec., with a film supply lasting one minute.

---

\* "Dynamic Measurements on the 81mm Shell M-56 in the NBS Wind Tunnel", Zarodny and Mott.

**OPERATION:**

WHEN THE MOTOR IS STARTED, THE CHAINS AND SPROCKETS DRIVE ALL FOUR STATIONS SYNCHRONOUSLY. ALL FRONT CRANKS ARE IN PHASE, SO THAT THE INTERSECTION OF THE FRONT WIRES MOVES ABOUT THE CENTER LINE OF THE TUNNEL IN A CIRCULAR PATH WITH A RADIUS EQUAL TO THE DISTANCE THE WIRE SUPPORTS ARE PLACED FROM THE CENTER OF THE CRANKS. THE REAR CRANKS ARE 180° OUT OF PHASE WITH THE FRONT CRANKS, SO THAT THE RESULTING MOTION OF THE MODEL FASTENED BETWEEN THE TWO WIRE INTERSECTIONS IS ONE OF CIRCULAR YAWING.

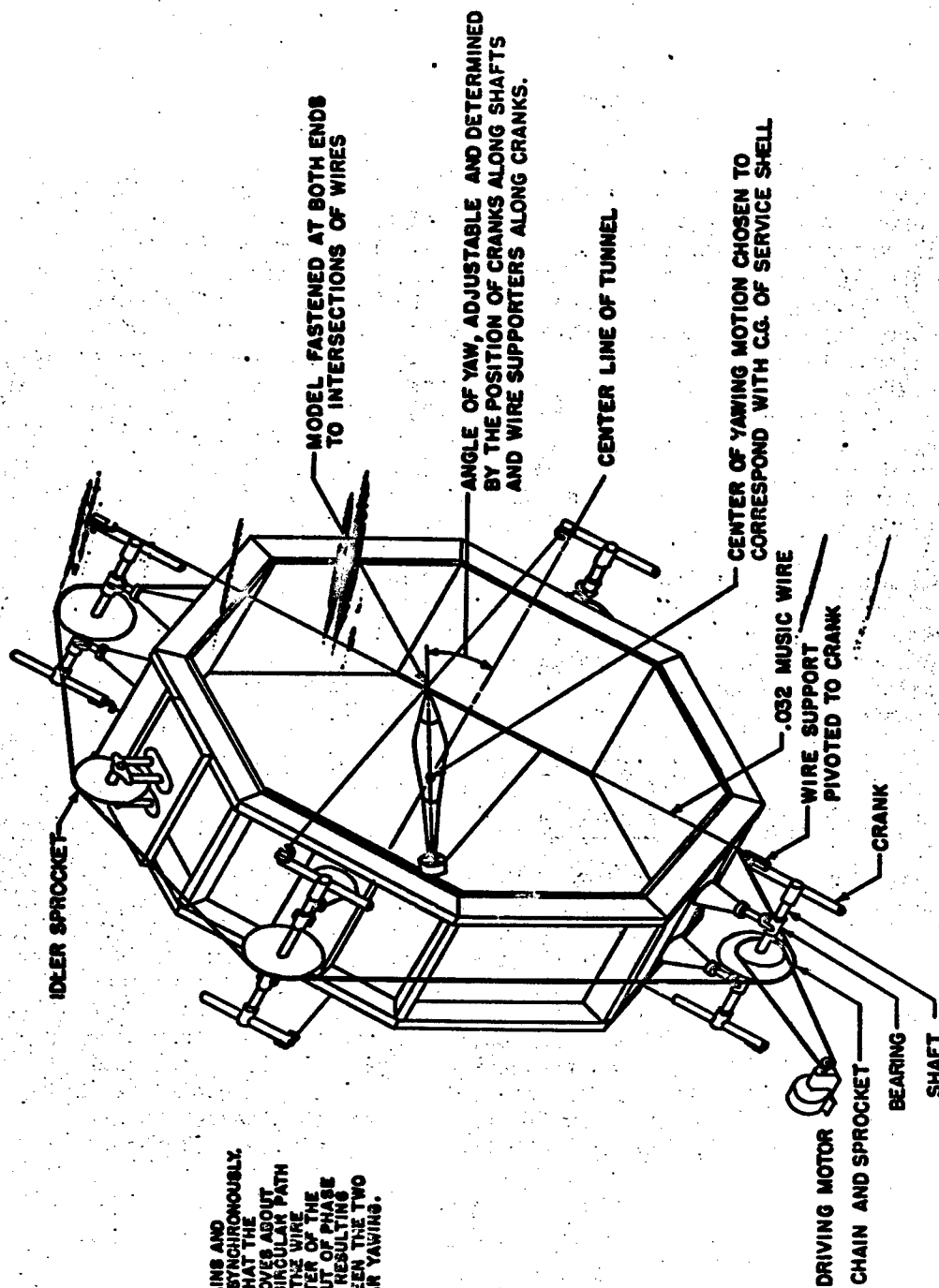


**FIG. 1 THE BRL-NBS RIG FOR THE GENERATION OF CIRCULAR YAWING MOTION**

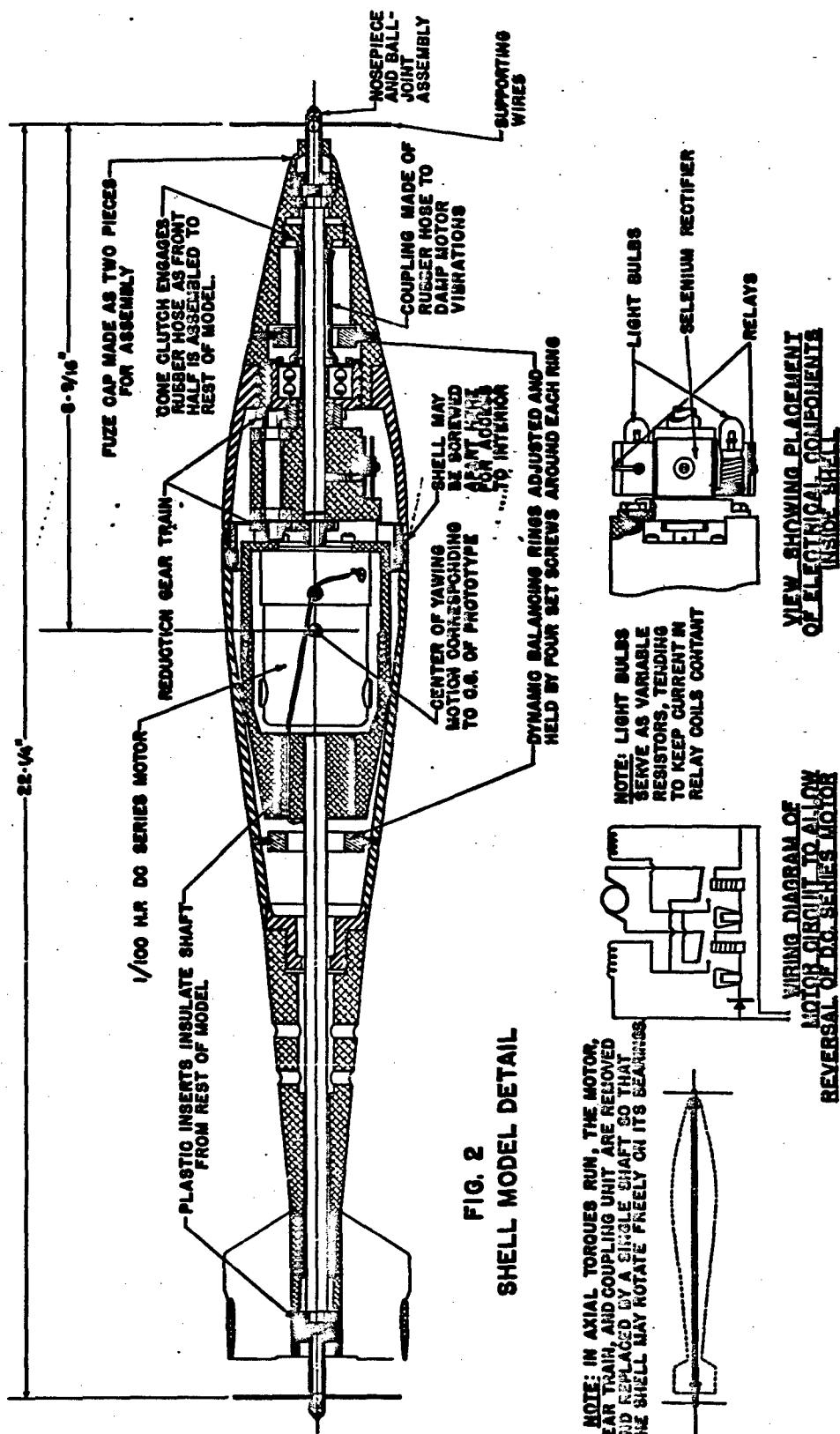
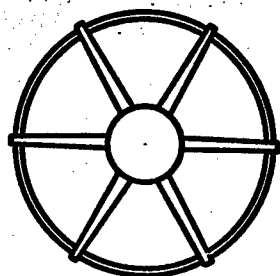
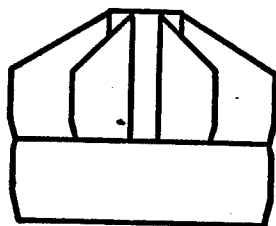
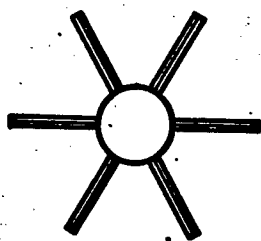
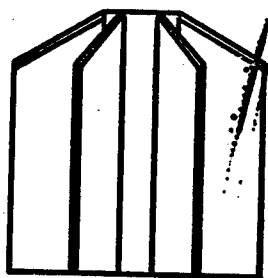


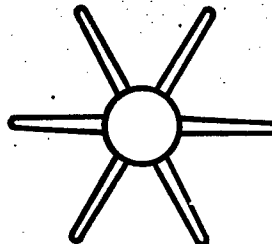
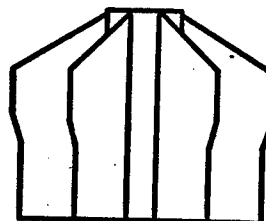
FIG. 2  
SHELL MODEL DETAIL



STANDARD FIN  
(DRAWING NO. 7-2-452)



LONG FIN



SHROUDLESS STANDARD FIN  
(SAME AS ABOVE WITH SHROUD REMOVED)

SCALE: 0 1" 2" 3"

FIG. 3

FIN TYPES USED IN TESTS

From theoretical considerations\* and experience with the M-56 data, the expression for the total axial torque was assumed to be a Maple-Synge expansion of the form

$$(1) \text{ Torque} = (\rho d^3 u^2) \left\{ K_E - v K_A \right. \\ + \left[ (K_E' + K_B N) + v(K_X + K_I N^2) \right] \sin^2 \delta \\ \left. + \left[ (K_E'' + K_1 N + K_2 N^3) + v(K_3 + K_4 N^2 + K_5 N^4) \right] \sin^4 \delta \right\}$$

where  $\rho$  is the density of the air,  $d$  the diameter of the shell,  $u$  the airspeed,  $v$  the spin in radians per caliber of travel,  $N$  the circular yawing rate in radians per caliber of travel, and  $\delta$  the angle of yaw. The expression  $\rho d^3 u^2$ , using consistent units, gives the dimensions of torque. All other coefficients and variables are dimensionless.

Although the individual terms of the above expansion are arrived at largely through mathematical considerations and need not correspond exactly to separate concepts abstracted from the general axial torques phenomenon, certain associations are made between some of the terms and the physical processes to which they are evidently related. Thus, the  $K_E$  series is associated with twisted fins;  $K_B$  is associated with the unequal lift given to fins in circular yawing due to body interference, which generates spin in the same sense as the yawing; and  $K_A$  is generally thought of as representing the spin damping due to the viscous air resistance, and also (in the case of finned shell) due to the effective angle of attack and the resulting lift forces on the fin blades incurred by a fin spinning in an axial airflow. The other terms are interpreted as being the mathematically allowable extensions of these effects to the higher orders of  $N$  and  $\delta$ , the importance of the terms diminishing with higher order.

From the angular displacement vs time record of the shell subjected to the axial torques, as read from the motion picture film, the angular velocity,  $\dot{\theta}$ , and the angular acceleration,  $\ddot{\theta}$ , may be determined by numerical differentiation. Obviously,  $\dot{\theta}$  is proportional to the spin,  $v$ , and  $\ddot{\theta}$  is proportional to the axial torques generating the spin.  $\ddot{\theta}$  is plotted against  $\dot{\theta}$ , and a straight line is fitted to the data (with certain corrections noted below). The intercept of this line on the  $\dot{\theta}$  axis is proportional to the group of terms in (1) independent of  $v$ , and the slope of the line is proportional to the group of terms dependent on  $v$  (see Fig. 4). Thus from each film there may be obtained two numbers, the intercept and the slope, each representing a group of six terms.

\* K. L. Nielsen and J. L. Synge, Q. Appl. Math., 4, 201-226 (1946).

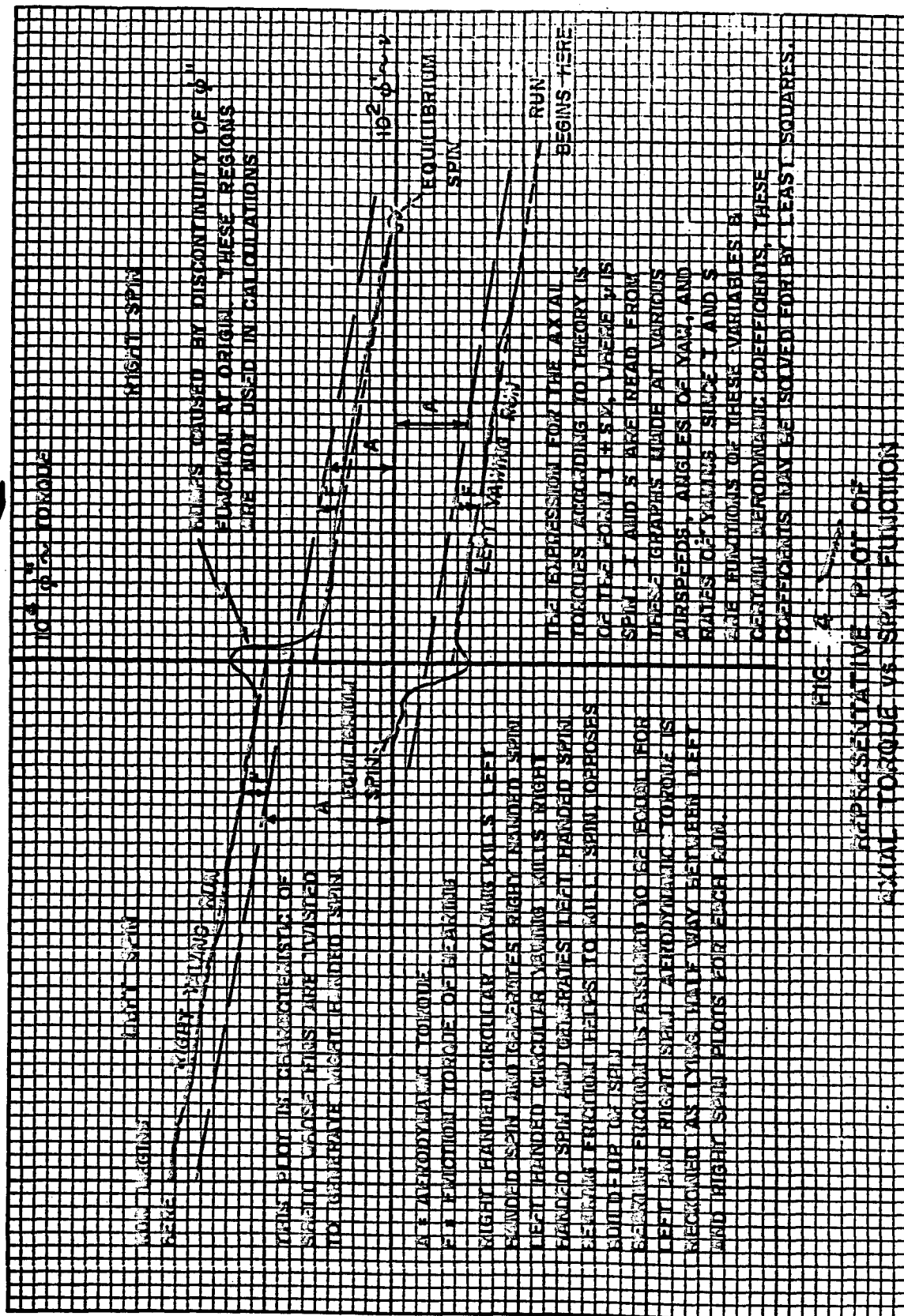


FIG. 4  
REPRESENTATIVE PLOT OF  
AXIAL TORQUE VS. SPIN FUNCTION

To solve for the coefficients of these terms one must have at least six independent pairs of numbers (equations in six unknowns). In practice, the results of eighteen runs were used in the least squares solution for these coefficients. Runs were made at yaws of 5, 10, 15 and 20 degrees, at airspeeds of 100 and 200 fps, and with circular yawing rates of .495 cycles per second in both left and right handed directions. The yawing rate and airspeed combine to give N of .0082 and .0041 radians per caliber\*. Runs made from these combinations of  $\delta$  and N make an overdetermined set as far as the intercept reduction is concerned; but in order to make the set determinate for the slopes (which do not distinguish between positive and negative values of N) it was necessary to include runs at a third N value, so runs were also made at 20°, 100 fps, left and right spin at N = 0.

All runs were begun with the shell spinning counter to its circular yawing\*\* so that the spin accelerating, spin damping, and bearing friction torques would combine to create a large spin retardation and thus provide a longer  $\phi''$  vs  $\phi'$  plot within the one minute duration of the run. Depending largely on the magnitude and direction of the  $K_2$  effect, spin reversal might or might not occur within the time of the run. It was desirable that spin reversal occur in enough instances to give an estimate of the bearing friction, which appears as an offset between the parallel left and right-hand branches of the  $\phi''$  vs  $\phi'$  plot and has to be known to correct for the intercepts in those instances where spin reversal does not occur. Generally, the runs in which reversal occurred gave inferior estimates of the slopes because of their shortness and their roughness near the  $\phi''$  axis (where the differentiating operation blends the offset left and right spin regimes). This region is disregarded in the estimates.

The slopes and intercepts of the plots were read by eye with the aid of a straightedge, the computer making the best guess under the circumstances. The computer also estimated the possible range within which each slope might fall, and thereby obtained a measure of the degree of certainty

---

\*  $N = 2\pi$  (cycles/sec.) d/u. These yawing rates were originally chosen to bracket the natural yawing rate for the M-56 shell in the considered airspeed and yaw ranges. To expedite the T-28 tests, which were closely scheduled to fit in before the impending tunnel alterations, the same gearing was utilized for the yawing mechanism as before, on the expectation that the natural yawing rate for the T-28 would not be too far off from that for the M-56. From information subsequently available, it was found that the yawing period for the T-28 is less than half of that for the M-56 (138 ft. vs 322 ft. respectively), so that to bracket the natural yawing rate the shell should have been yawed twice as fast. Measurements were made at three N values (the third being zero), however, which provide a good basis for such a short extrapolation.

\*\* Spin was induced either by circular yawing or by a jet of air directed against the fins with an airhose prior to the run.

with which each slope was read. The range values were assumed to be proportional to the standard deviations and were handled as such in the computing of the relative weights of the slopes and intercepts. Thus, tables of slopes and intercepts, with their relative weights, were obtained as functions of the variables  $N$  and  $\delta$ , from which the various aerodynamic coefficients contained in the slopes and intercepts were solved for by the method of least squares.

## B. Results

As noted in the introduction, tests were made on the T-28 with the standard fin, a shroudless standard fin, a long, high area fin, and a finless tail boom (see Fig. 3). The results of these axial torques tests are shown in Fig. 5 (Intercepts and Slopes as Functions of Yaw), and in Fig. 6 (Aerodynamic Coefficients of Axial Torque). Data from the finless shell are not included since no axial torques other than a very weak  $K_A$  effect were discernible in tests of this configuration. In Fig. 5, the intercepts and slopes are scaled so that they represent those dimensionless groups of terms in the axial torques expression which are independent of  $v$  and dependent on  $v$ , respectively. The curves drawn are the least squares fits to the data points. The radii of the circles around the data points are proportional to the individual ranges of the points. Weights given to the points in the least squares reduction were proportional to the inverse of the ranges squared.

In the intercept graphs,  $K_E$  is the offset in the curves from the origin, while  $K_E'$  is responsible for the lack of rotational symmetry between the left-spin and right-spin curves.  $K_E''$  was not computed since its effect was expected to be small. The  $K_E$  group is of interest here in that it "absorbs" the effects of bent fins and the spirality of the airflow in the tunnel. The values of  $K_E$  and  $K_E'$  should not be considered as representative of the general fin configuration from which they were obtained; apparently they are characteristic of the particular fin sample used and the wind tunnel in which the tests were made.  $K_B$  is represented by the slope of the curves at the origin and  $K_1$  and  $K_2$  are responsible for the curvature.

In the slope graphs, no distinction is made between left  $N$  and right  $N$  since all terms allowed in the slope expression are even in  $N$ . The points shown are averages of the left and right  $N$  slopes.  $K_A$  shows up as the intercept of the slope curve,  $K_X$  and  $K_Y$  in its slope at the origin, and  $K_3$ ,  $K_4$ , and  $K_5$  in its curvature.

In these tests the intercept data turned out to be rather poor, since the intercepts were obtained either from short, rough,  $\phi'$  vs  $\phi''$  curves near the origin or from larger, smoother curves far removed from the origin and requiring a large amount of extrapolation. The slope measurements did not require such extrapolation and turned out to be quite good. The scatter

in the intercept data, however, does not obscure certain qualitative relationships that can be observed from the results as a whole. The general trend is for the intercept, or "spin generating function", to be largest in the  $15^\circ - 20^\circ$  region of yaw, while the slope, or "spin damping function", is a minimum in this region. Although the maximum intercept values reached within the  $20^\circ$  yaw range of the tests are roughly the same for all fin types tested, the standard fin intercept plots have the greatest curvature,\* reaching its maximum at  $15^\circ$  and then dropping rapidly to zero at  $20^\circ$  for the 100 fps runs. The intercept plots for the other fins are more nearly linear. In the slope curves, the standard fin again shows the greatest non-linearity in yaw, and gives the least resistance to spin in the middle yaw regions for the three fins tested. Thus the striking differences observed in these tests are between shrouded and non-shrouded fins, the differences between the two shroudless fins being largely matters of degree.

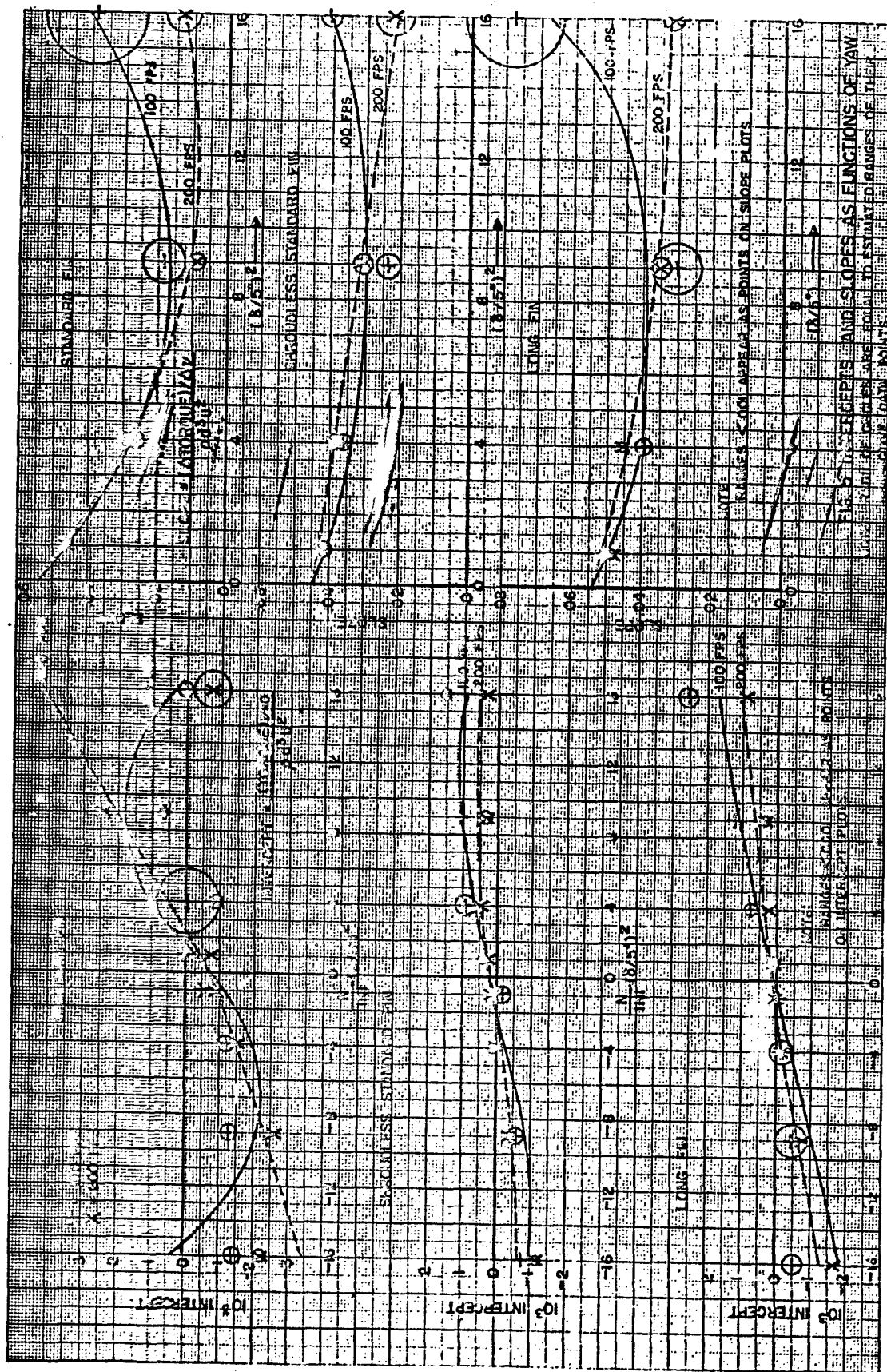
A possible interpretation of the above observations based on our previous understanding of the axial torques phenomena is as follows. As mentioned earlier, the  $K_B$  and  $K_A$  effects may be explained in terms of lift or normal force acting on the individual fin blades. This concept may be extended to include the effects of the higher order terms in  $\delta$  of (1) by considering how the normal force on the fin blades may vary with increasing yaw. Following this line of thought, we should expect the  $K_B$  effect, which does not exist at zero yaw, to increase with yaw until some optimum yaw is reached at which the lift differential due to body interference is a maximum, and then diminish as the fins are moved outwards from the wake of the shell body with a further increase in yaw.

The  $K_A$  effect should be a maximum at zero yaw where all the fin blades contribute equally to spin damping through lift, and should diminish at higher yaws where interference effects of the blades and boom reduce the effectiveness of the fin as a whole. At higher yaws, however, the normal force on the fins begins to build up again largely through drag.

This buildup may be visualized by considering a spinning fin set at right angles to the airflow. The blades on one side of the yaw plane advance into the airflow and the blades on the opposite side recede from the airflow, creating an unbalanced blade drag distribution whose axial moment is proportional to the product of the spin and airflow (whose torque, we see, is of the form of the slope terms). The resultant spin damping effect for any angle of yaw then is essentially the sum of these two aspects which have their maxima  $90^\circ$  apart, and may readily account for the slope curve characteristics observed from these tests\*\*

\* The reader is asked to observe the position of the data points in this instance rather than the least squares curves. As a consequence of our weighting procedures, the 200 fps data seems poorly fitted by the least squares method in this case.

\*\* These effects would be more easily perceived if the slopes were plotted against  $\delta$  instead of  $\delta^2$ , since in the latter case the maximum at zero yaw appears cusp-like.



$$\text{Axial torque} = \rho d^3 u^2 \sum_i K_i (\text{factor})_i \text{ foot-pounds}$$

Values in parenthesis are estimated standard deviations of the fit in terms of the value of the coefficient.

	Coefficient	Factor	Standard Fin	Shroudless Standard Fin	Long fin
from intercepts	$K_E$	1	-.000,747(21%)	+.000,231(20%)	+.000,119(62%)
	$K_E'$	$\delta^2$	+.0091(44%)	-.0021(48%)	-.0019(76%)
	$K_B$	$N\delta^2$	+ 7.89(23%)	+ 2.51(18%)	+ 1.99(37%)
	$K_I$	$N\delta^4$	+ 19. (148%)	- 10. (61%)	+ 4. (177%)
	$K_2$	$N^3\delta^4$	- 1,245,000(24%)	- 43,000(133%)	- 89,000(119%)
from slopes	$K_A$	$\rightarrow$	+ .0537 (1%)	+ .0442 (4%)	+ .0539 (2%)
	$K_Y$	$v\delta^2$	+ .981 (5%)	+ .114 (150%)	+ .279 (30%)
	$K_Y'$	$vN^2\delta^2$	+ 1,960 (60%)	+ 4,880 (60%)	+ 5,120 (38%)
	$K_3$	$v\delta^4$	- 7.46 (6%)	- .68 (214%)	- 1.86 (38%)
	$K_4$	$vN^2\delta^4$	+ 154,000(13%)	+ 61,000(99%)	+ 45,000(57%)
	$K_5$	$vN^4\delta^4$	- 2.47 x 10 <sup>9</sup> (12%)	- 1.50 x 10 <sup>9</sup> (53%)	- 1.58 x 10 <sup>9</sup> (23%)

Fig. 6 Aerodynamic coefficients of axial torque

The difference observed between the shrouded (standard) fin and the non-shrouded ones with respect to these data may be explained by the shroud's role as a tip plate for the fins and its interference effect upon the fin blades at high angles of yaw. The effect of the addition of tip plates on lift sections of low aspect ratio is markedly to increase the airfoil's lift, so with the addition of a shroud to a given fin, we should expect an increase in those axial torques which are essentially manifestations of lift acting on the individual fin blades. Indeed, we find that both the  $K_B$  and  $K_A$  effects are most pronounced in the case of the shrouded fin (see Figs. 5 and 6). Of the fin types tested, the shrouded fin has the greatest  $K_B$  (by a factor of 3) and its  $K_A$  is as great as that of the high area long fin. The addition of a shroud further complicates the picture in that at increasing angles of yaw the shroud begins to nullify the effectiveness of the fin blades through interference. This is indicated by the fact that for the standard finned shell the intercept plot has the greatest negative curvature in yaw; and the slope plot, although having one of the highest values at zero yaw, quickly drops to a value lower than that for any other fin by 10 degrees of yaw.

The results of the T-28 axial torques runs are generally comparable to those made on the M-56 shell, although the differences between shrouded and non-shrouded fins were slight in the M-56 runs. The comparison was obscured in those runs by the fact that the shroudless fin was 12 bladed and the shrouded fin was 6 bladed, so that they were not comparable on the basis of the shroud alone.

## II. MAGNUS TORQUE

### A. Instrumentation and Data Reduction

A schematic sketch of the Magnus torque balance is shown in Fig. 7. For a more detailed description of the balance, see ERL 882. The balance used in the present runs differs only slightly from the one used in the M-56 runs. The knife edges used in the fulcrums and end pivots of the old balance have been replaced by thin metal flexure plates (see Fig. 8), thereby lessening the problems of friction and "stickiness" (failure of the balance to return to its original position upon the removal of a displacing torque) associated with the knife edge set-up without appreciably increasing the stiffness of the system. In order to increase the sensitivity of the balance by counteracting the strong stabilizing influence of the taut cross-wires, the fulcrums of the balance beams were shifted 2" inwards towards the shell from the level of the end supports, thus creating a condition of instability similar to that of a pyramid supported on its point. This method of sensitizing or de-stabilizing the balance is superior to the method used in the M-56 runs, in which a 20 lb. weight was attached to the upper balance beam some two feet above its fulcrum, an arrangement which was cumbersome and necessitated an additional adjustment with each change of yaw.

To determine Magnus torque as a function of the pertinent variables yaw and spin, runs were made at yaws of 5, 10, 15 and 20 degrees\*, at airspeeds of 50, 100, and 200 fps, and at spins from 600 to 2400 rpm, at 200 rpm intervals. These last two variables combine to give  $v$  ranges from .083 to 1.328 radian/cal. A run consists of a series of 10 Magnus torque measurements taken at 10 spin values for a constant airspeed and angle of yaw. Torques are measured on the balance by noting the position that a known weight must occupy along the graduated upper balance beam in order to hold the balance beams in their neutral positions (i.e., the positions in which the model has no yaw in the balance plane), as shown by the position of a light spot on a screen (see Fig. 7). Magnus torque is reckoned as the difference between torque measured at zero spin (the "zero reading") and torque measured at the desired spin (the "spin reading"), for a given airspeed and angle of yaw. Zero readings were made directly before each individual spin reading, since the zero readings have been observed to drift considerably during the same 30 minutes length of a run. Otherwise some average zero reading could have been applied throughout in the computations.

As an extension of the linear theory and for the convenience of least squares computations, Magnus torque is considered as an odd term Taylor expansion of the following form:

$$(2) \quad T = \rho d^3 u^2 \left[ K_{T_{11}} v \delta + K_{T_{13}} v^3 \delta + K_{T_{15}} v^5 \delta + K_{T_{31}} v \delta^3 + K_{T_{33}} v^3 \delta^3 + K_{T_{35}} v^5 \delta^3 + K_{T_{51}} v \delta^5 + K_{T_{53}} v^3 \delta^5 + K_{T_{55}} v^5 \delta^5 \right]$$

where the  $K_{T_{ij}}$  are, of course, numeric and the other quantities are as noted for expression (1) in part IA (with  $\delta$  here restricted to radians).

The  $K_{T_{ij}}$  were not computed directly in the usual least squares manner since it was desirable to perform the reduction step-wise in order to examine the data more thoroughly and obtain visual checks throughout, but the resulting coefficients are identical to those that would be obtained from the direct approach. To express all measurements in terms of a common airspeed, all torques were multiplied by the factor  $\left(\frac{100}{u}\right)^2$ . All runs made at the same angle of yaw were combined and fitted as a group by a least squares, odd term, fifth-order polynomial in  $v$ . Fig. 9 shows the Magnus torque measurements as a function of spin for the standard fin T-28 at 15° yaw, with the

\* Repetition of runs at negative angles of yaw as done in the exploratory M-56 tests was not considered necessary here.

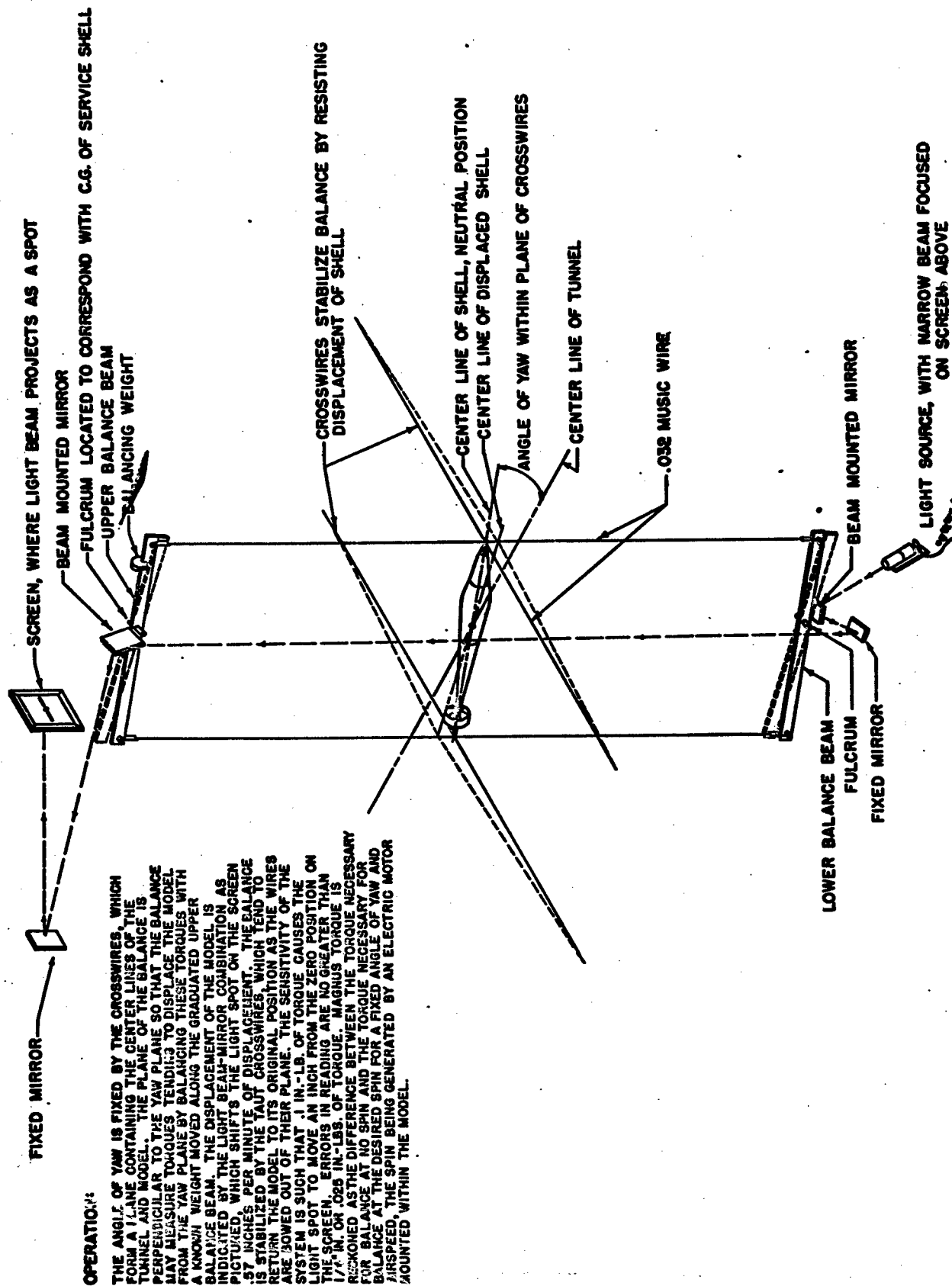
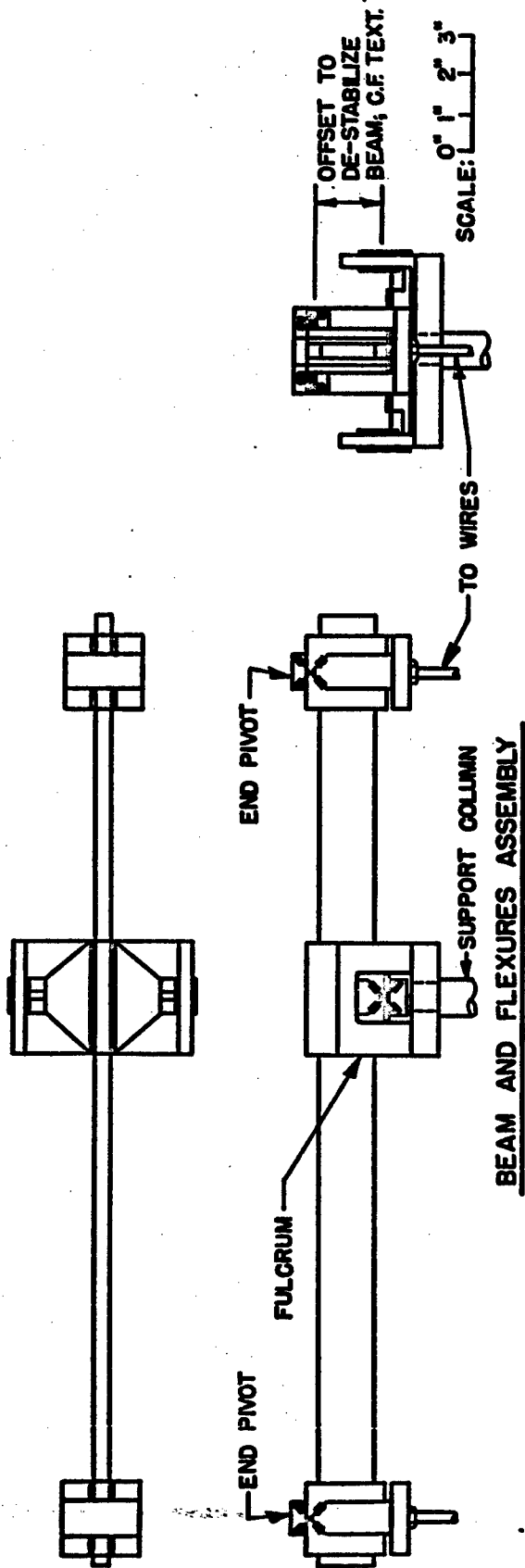
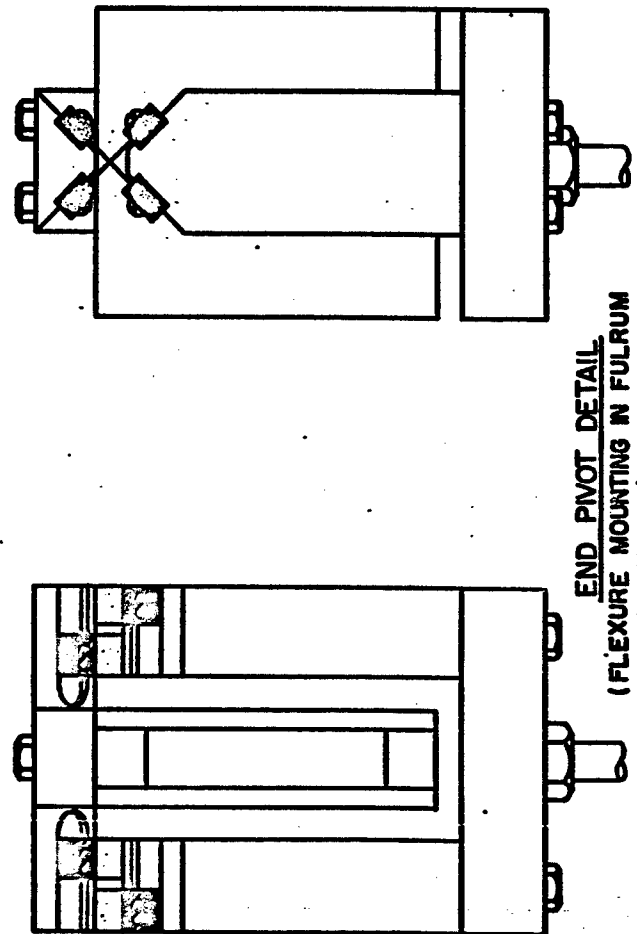


FIG. 7 SCHEMATIC OF THE BRL-NBS MAGNUS TORQUE BALANCE



NOTE: ALL FLEXURES ARE LOADED IN TENSION TO AVOID BUCKLING.



**FIG. 8**  
BALANCE BEAM DETAIL

least-squares fit drawn in. Again, as with the M-56 data, a fifth order fit was necessary to describe the data adequately. Such fits were obtained from all four angles of yaw, yielding the expressions for Magnus torque:

$$T_{5^0} = b_5 v + d_5 v^3 + f_5 v^5$$

$$T_{10^0} = b_{10} v + d_{10} v^3 + f_{10} v^5$$

$$T_{15^0} = b_{15} v + d_{15} v^3 + f_{15} v^5$$

$$T_{20^0} = b_{20} v + d_{20} v^3 + f_{20} v^5$$

The  $b_i$ ,  $d_i$ , and  $f_i$  are then fitted by least squares, odd term, fifth order polynomials in  $\delta$ , giving the expressions:

$$b = B_b \delta + D_b \delta^3 + F_b \delta^5$$

$$d = B_d \delta + D_d \delta^3 + F_d \delta^5$$

$$f = B_f \delta + D_f \delta^3 + F_f \delta^5$$

It can be shown, providing that torque readings were made at the same set of spin rates for all angles (as was done in these tests), that

$$B_b = K_{T_{11}}; B_d = K_{T_{13}}; B_f = K_{T_{15}}$$

$$D_b = K_{T_{31}}; D_d = K_{T_{33}}; D_f = K_{T_{53}}$$

$$F_b = K_{T_{51}}; F_d = K_{T_{53}}; F_f = K_{T_{55}}$$

where the  $K_{T_{ij}}$  are the coefficients of the direct least squares fit to (2).

## B. Results

Before considering the overall results of these tests, certain peculiarities noticed in the individual runs should be examined for the information they contain -- unexpected irregularities in the tests which would have gone unnoticed in a direct least squares fitting of the data.

One of the most noticeable and puzzling features of the torque vs  $v$  plots for constant yaws (Fig. 9) is the large difference in torque values obtained between the left spin and right spin runs. In the previous work, similar (though smaller) discrepancies were dismissed by assuming that the airstream did not lie within the supposed plane of yaw, so that higher order components of righting torque, due to spin and even in spin, enter into the measurements. The asymmetry of airflow and the misalignment are known to be low, however, and computations show that, allowing a large asymmetry, no reasonable value of righting moment due to spin can account for the differences observed in these runs\*. Another possible cause, the effect of which is difficult to evaluate, may be that the wake of the front support wire does not wash down exactly along the leading edge of the model, thereby producing an aerodynamic asymmetry whose interplay with the Magnus effect may produce large differences between the left spin and right spin torque readings. The interference effect of wires in or near the plane of yaw is already suspect in causing autorotation of firmed models (as indicated from preliminary tests made in the NBS rig), and may be to blame in this case as well.

Another irregularity evident in these plots is the scatter within each individual run. Actually, the precision of measurement is much greater (.025 in.-lb. maximum error of reading) than is indicated by the scatter. In analyzing the data it was seen that the scatter was in the zero readings. This scatter may perhaps be attributed to the random orientation of the fins with respect to the yaw plane. The fins, in positions asymmetrical with respect to the yaw plane, may cause unbalanced forces acting out of the yaw plane, resulting in a "quasi-Magnus" force and torque. This explanation is supported by the fact that the Magnus torque runs made on the finless shell gave much smoother plots. It has long been recognized that righting torque is a function of fin orientation, but the "quasi-Magnus" torque variation with fin orientation has received less attention. In future runs, care should be taken to make all zero readings at some "average" or "representative" orientation of the fins throughout the runs.

It was decided that the ordinary least squares fit to the common yaw groups handled these data best. The differences between the left spin and right spin runs logically should not exist in the function we wish to represent, so it seems reasonable to assume that the true values of the function lie somewhere between the left and right spin plots. The least squares fit, using an odd term polynomial in spin, effectively averages these values. The scatter due to the fin orientation effect is considered to be random and likewise is best handled by the least squares.

---

\* Eg., if the misalignment is  $3^\circ$ , the righting moment due to spin must be approximately 57 times the Magnus moment to give the observed differences.

A summary of the data on the T-28E6 shell appears in Fig. 10, where the least squares polynomial fit is given in both tabular and graphical form. The torque vs spin graphs for constant yaws are almost identical to the least squares fits to the common yaw groups (as in Fig. 9) from which the overall fit was determined, and therefore give a good picture of the distribution of the original data. The torque vs yaw graphs for constant spins are more relevant in the study of yawing motion, since  $v$  values may generally be regarded as varying only slowly along the trajectory. As with the M-56 shell, Magnus torque was found to be non-linear both in spin and yaw. The data on the T-28 shell are generally comparable with those on the M-56 shell, although the torque readings from the T-28 are smaller than comparable readings from the M-56, as one would expect from a smaller shell (20% less body surface area). Thus, the belief that the non-linear Magnus torque characteristics of the M-56 shell were due to its particular shape does not seem to be tenable.

The results of the Magnus torque tests made on the T-28 with the shroudless standard fin, the long fin, and the finless shell are presented in Figures 11, 12 and 13 respectively. Comparative plots of the torque vs spin characteristics for individual yaws are offered in Fig. 14. From the comparison of these results, two patterns which were evident from the M-56 tests are again apparent: (a), the Magnus force contribution of the fins is negative for yaws below 20 degrees, and (b), the shroud increases the effectiveness of the fins in generating Magnus force. The effect of fins for yaws of 5, 10, and 15 degrees is to make the Magnus torque more positive, indicating that their force contribution must be negative in these regions since the fins have a negative moment arm. At 20 degrees yaw, the effect of the fins is to make the Magnus torque more negative. These effects are most pronounced for the standard fin (shrouded) and the high-area long fin.

In an attempt to explain these findings, the following hypothesis is suggested. Consider a typical multi-bladed fin spinning in an axial air-flow. Because of the rotation of the fin, each blade will have an effective angle of attack and resulting lift force. Because of symmetry, the vector sum of these forces is zero, with only the spin damping  $K_A$  moment surviving. Now consider the fin spinning at an angle of yaw. With respect to the yaw plane, the force system is no longer symmetrical because the lift on the sheltered leeward blades is less than that on the windward blades, hence the resultant of all the individual blade forces will be in a direction generally opposite to that of the motion of the windward blades with respect to the yaw plane\*. As the angle of yaw is increased to a value of 20 degrees or more, however, the fin presents more of its side

---

\* This is a more precise, though less concise, re-statement of the intuitive "paddling" concept forwarded in ERL 882. The term "paddling", however, emphasizes drag rather than lift with which we are here concerned. The addition of a shroud to a paddlewheel would obviously reduce its propelling power, yet here we wish to demonstrate what might appear to be just the opposite.

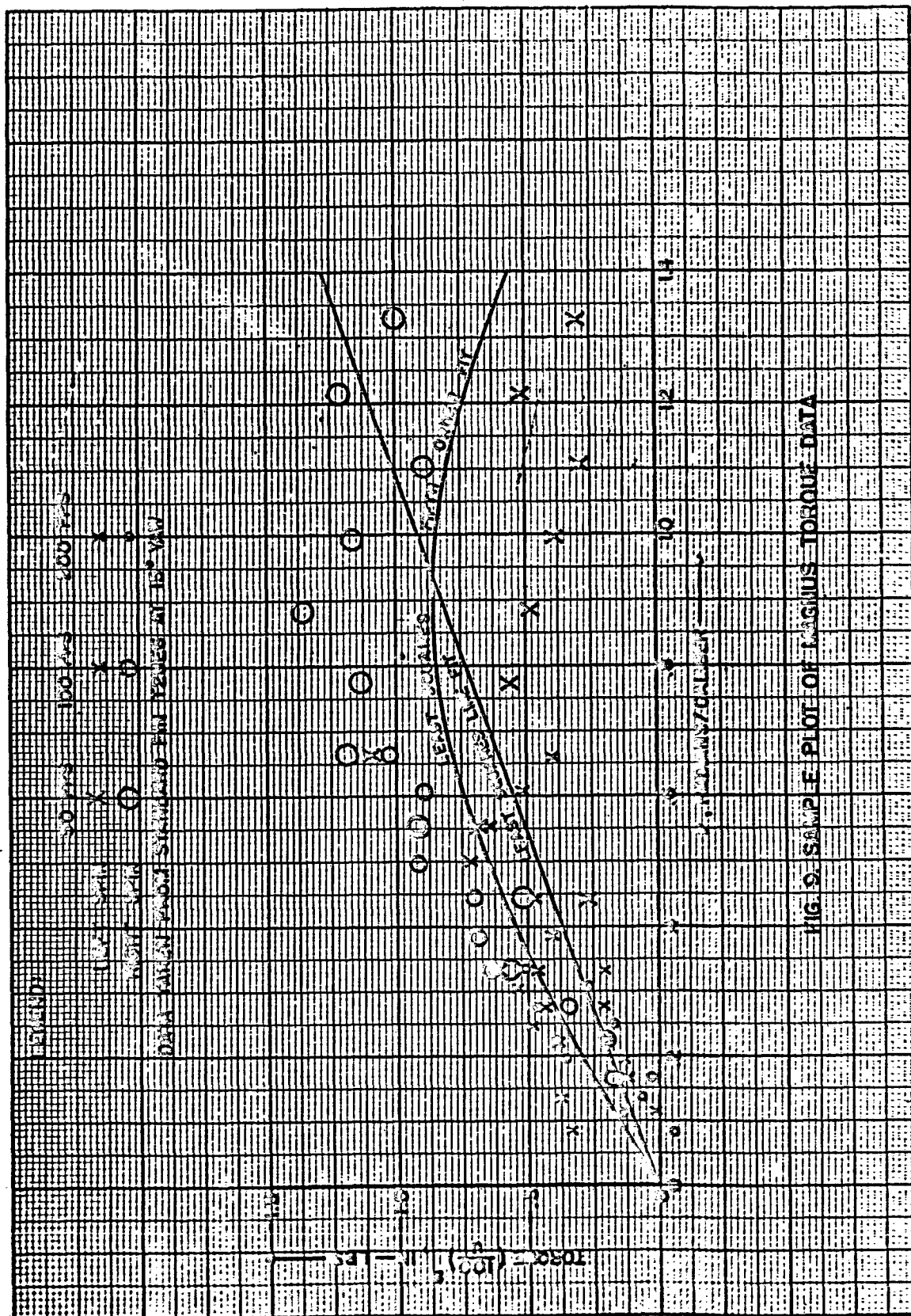


FIG. 9. SAMPLE PLOT OF MAGNUS TORQUE DATA

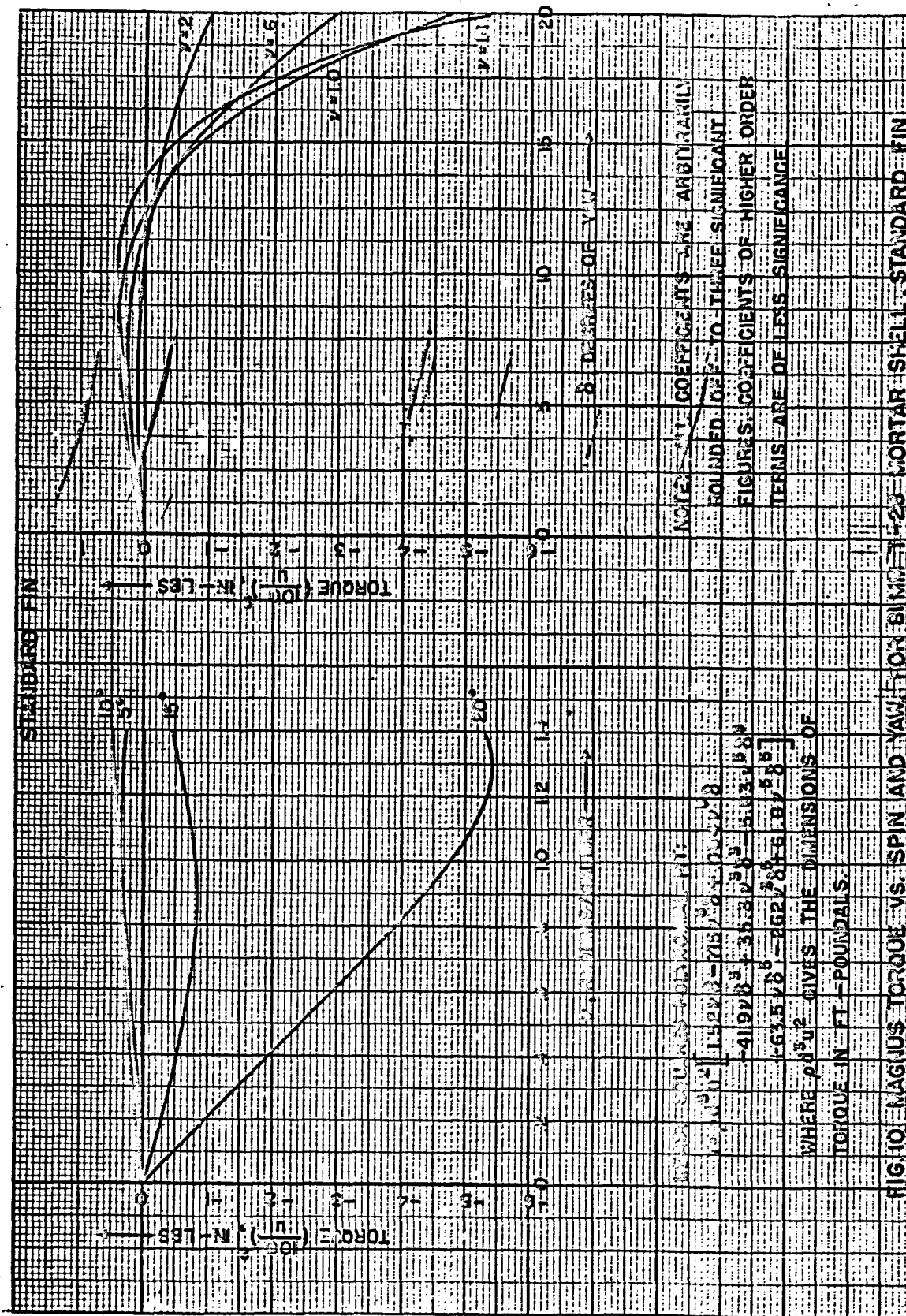


FIG. 10. MAGNUS TORQUE VS. SPIN AND YAW FOR CORTAR SHELL, STANDARD FIN

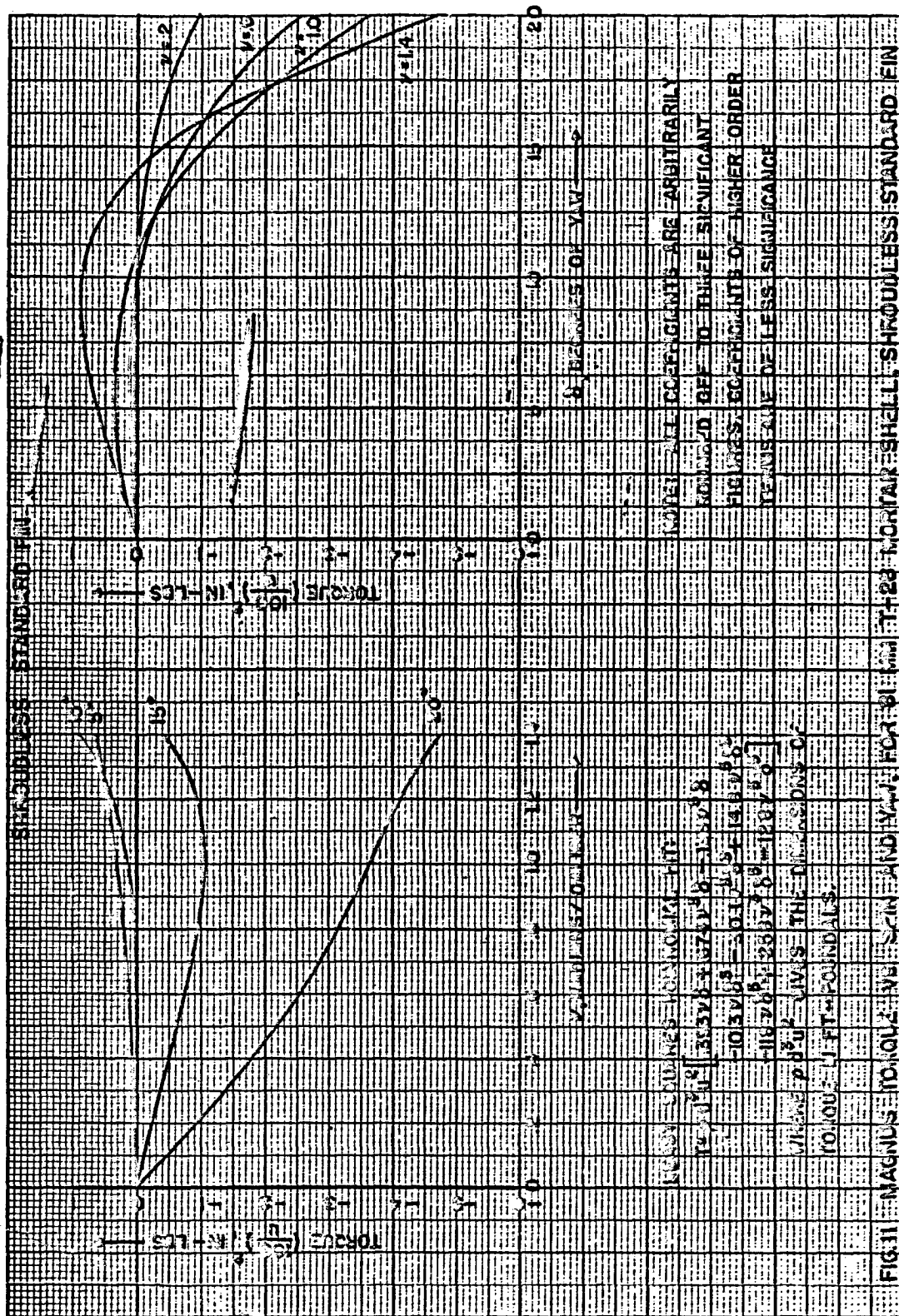


FIG. 11 MAGNITUDE OF TORQUE FOR YAW AND YAW RATE FOR A STANDARD SHIP

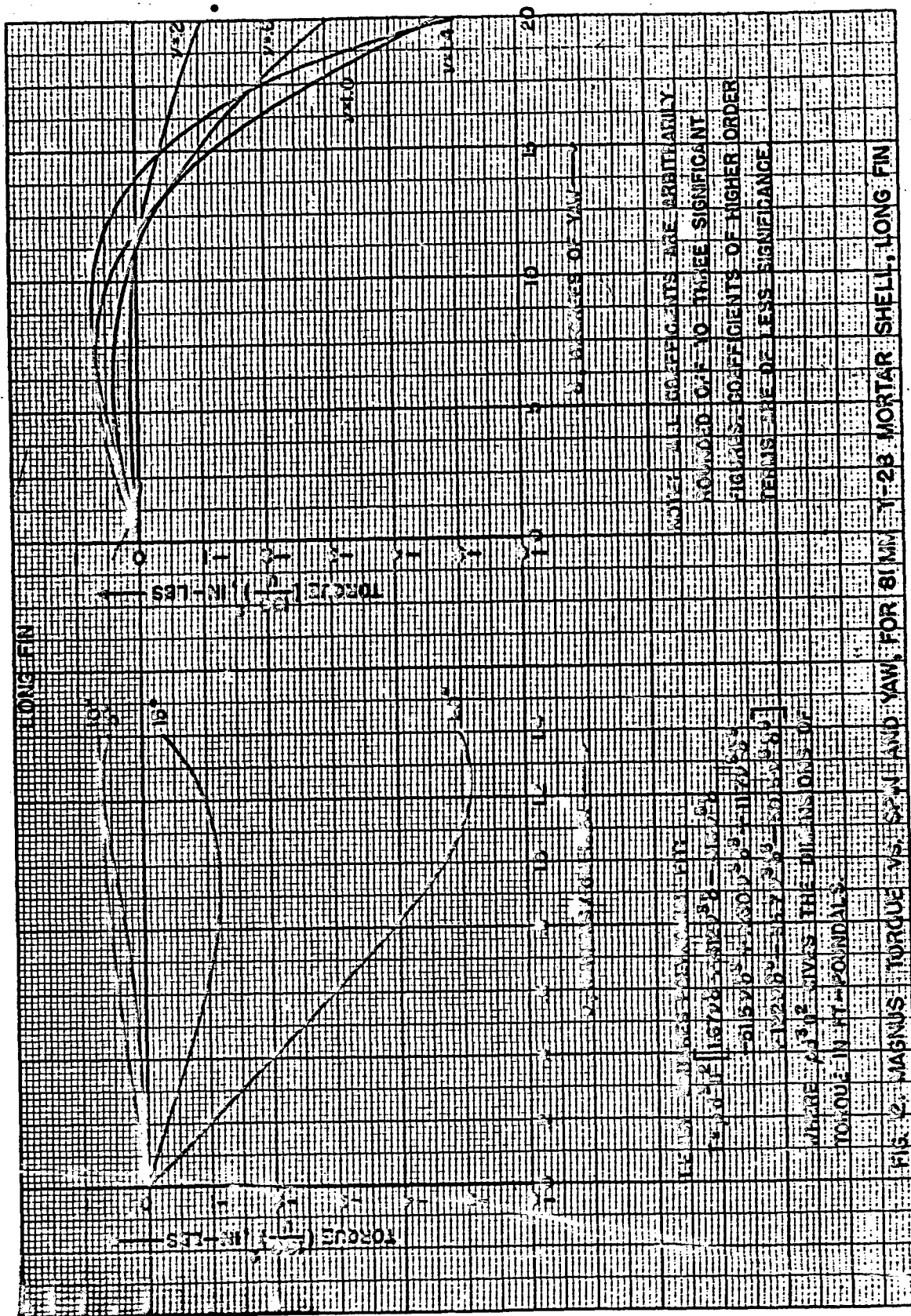


FIG. 2. MAGNUS TORQUE VS. SHELL YAW, FOR 81MM Y-23 MORTAR SHELL, LONG FIN

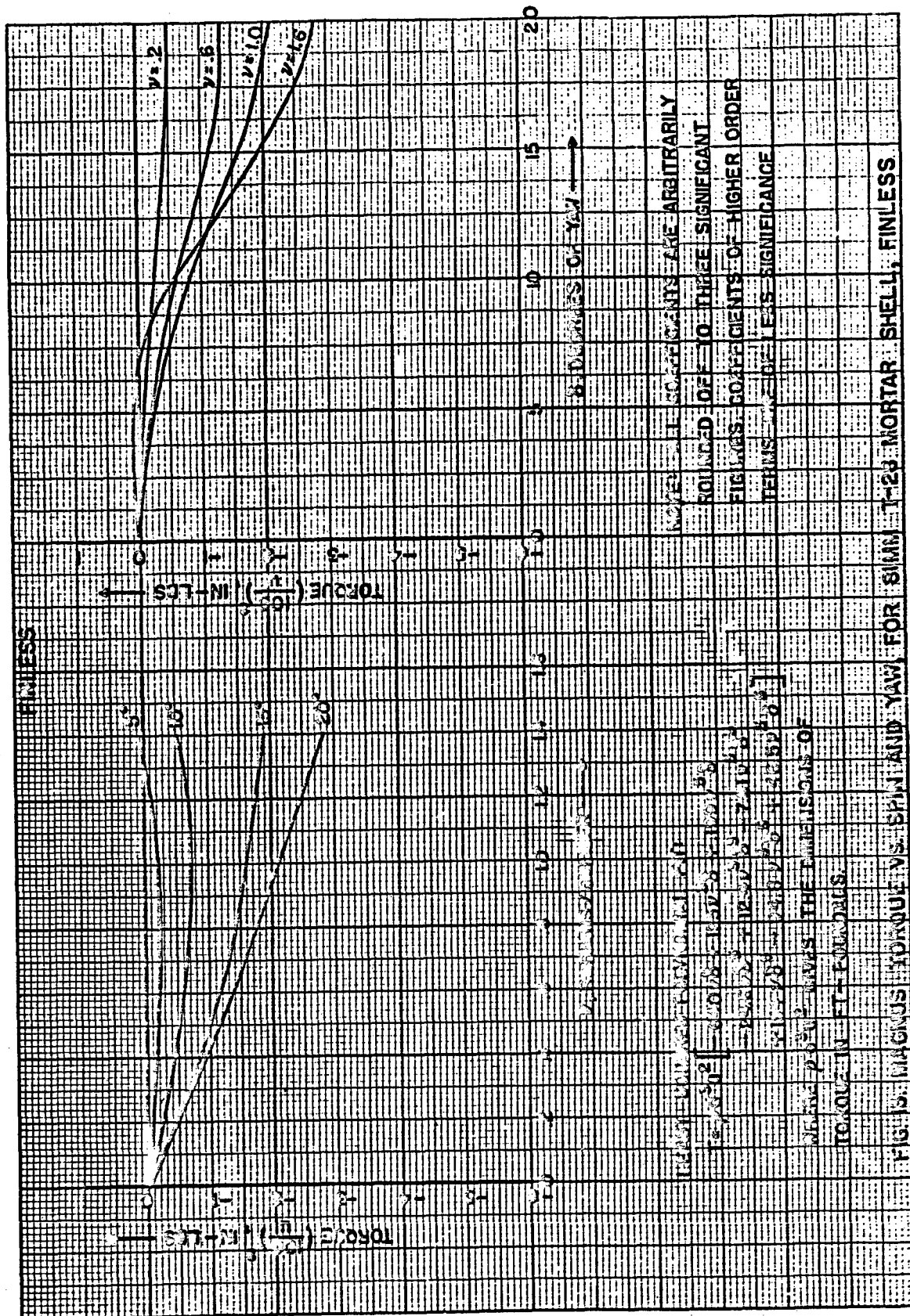


FIG. 5. MAGNUS TORQUE VS. SPIN AND YAW FOR 8mm T-23 MORTAR SHELL, FINLESS

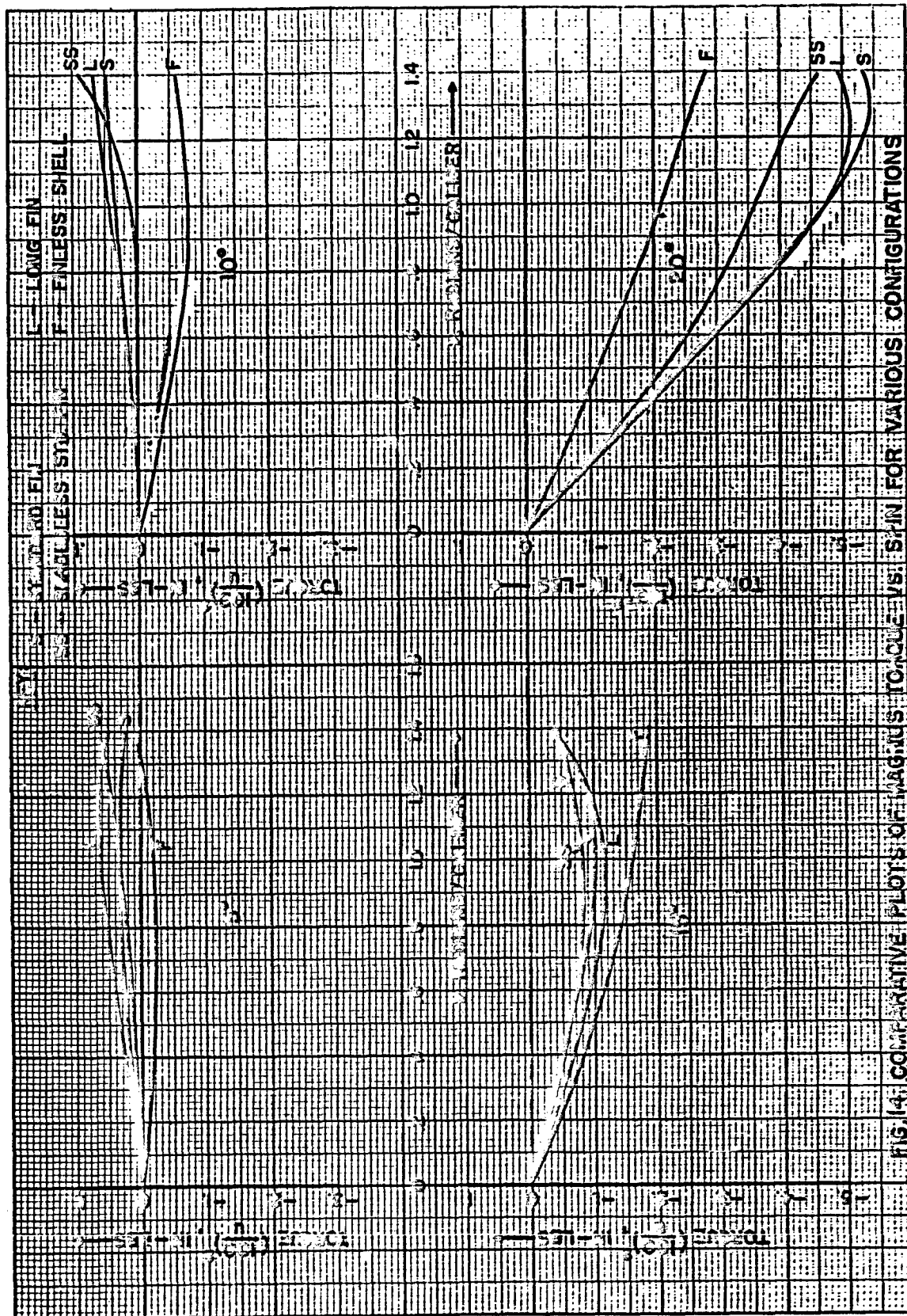


FIG. 14. COMPARATIVE PLOTS OF MAGNUS TORQUE VS. SPIN FOR VARIOUS CONFIGURATIONS

to the airstream which must now go around the fin as well as through it, so the spinning fin becomes in effect more of a body of revolution, and the usual viscous Magnus force (positive) outweighs the blade lift force. The larger the fin area, the more pronounced these characteristics are for a given shell body. The addition of a shroud to a given fin prevents tip losses (of lift) from occurring on the individual blades, thereby increasing their lifting power (as noted in Part IB) and the resulting negative Magnus force in the 0 to 15 degree yaw region where the airflow is largely axial with respect to the fin. At higher yaws, where the cross-flow becomes more important, the shroud, itself a short body of revolution, generates the usual positive Magnus force associated with shapes of this type so that the overall Magnus force effect is more positive than it would be at these angles without the shroud. The effect of the shroud, then, is to increase the effectiveness of the fins with respect to the Magnus phenomenon as though the fin blade area were increased.

#### CONCLUSION

As noted above, the data on the T-28 are very similar to those on the M-56 shell, especially with respect to the non-linear Magnus torque. In view of such similar results obtained from such dissimilar shell configurations, it seems likely that these characteristics are representative of mortar shell in general, rather than being due to some particular design feature of either shell. Furthermore, the fact that the fins contribute so heavily to both the axial and Magnus torques indicates that these results may be of significance to all finned missiles\*.

At present, the main value of this work, as supported by the results of the preceding tests, is in its indication of the need for a more inclusive theory of yawing motion than the existing linear theory. Upon the development of such a theory, and through the use of modern computing machines, comparative studies of the accuracy and susceptibility to short ranges of various shell will be possible using this sort of data. The non-linear equations of yaw have been solved in a special case of spiral yawing motions using values of Magnus torque taken from the M-56 tests\*\*, and a similar treatment of the T-28 data is planned.

*Robert S. Mott*

R. S. MOTT

\* At the time of this writing, reports of similar research from other agencies bear witness to the generality of these results.

\*\* BRLM 682, Spiral Yawing Motions of 81mm M56 Shell, S. J. Zarodny, E. E. Bomberger.

# DISTRIBUTION LIST

<u>No. of Copies</u>	<u>Organization</u>	<u>No. of Copies</u>	<u>Organization</u>
3	Chief of Ordnance Department of the Army Washington 25, D. C. Attn: ORDTB - Bal Sec (1 cy) ORDTA (1 cy) ORDTX-AR (1 cy)	1	Superintendent Naval Postgraduate School Monterey, California
10	British - ORDGU-SE, Foreign Relations Section for Distribution Of Interest to: Superintendent of External Ballistics Woolrich Arsenal British Supply Office ADD Mortar Panel, RRDE Attn: Dr. N. Simmons ARE, Attn: Mr. P.J. Dawson	1	Commandant Headquarters, Marine Corps Washington 25, D. C.
		2	Commander Wright Air Development Center Wright-Patterson Air Force Base, Ohio Attn: WCIG WGLSW
4	Canadian Joint Staff - ORDGU-SE, Foreign Relations Section for Distribution	5	Director Armed Services Technical Information Agency Documents Service Center Knott Building Dayton 2, Ohio Attn: DSC-SA
4	Chief, Bureau of Ordnance Department of the Navy Washington 25, D. C. Attn: Re3	3	Director National Advisory Committee for Aeronautics 1724 F. Street, N. W. Washington 25, D. C. Attn: Div. Research Information
4	ASTIA Reference Center Technical Information Div. Library of Congress Washington 25, D. C.	2	National Advisory Committee for Aeronautics Langley Memorial Aeronautical Laboratory Langley Field, Virginia
2	Commander Naval Proving Ground Dahlgren, Virginia	1	National Advisory Committee for Aeronautics Ames Laboratory Moffett Field, California Attn: Dr. A. C. Charters
2	Commander Naval Ordnance Laboratory White Oak Silver Spring 19, Maryland		
2	Commander Naval Ordnance Test Station Inyokern P.O. China Lake, California Attn: Technical Library		

# DISTRIBUTION LIST

<u>No. of Copies</u>	<u>Organization</u>	<u>No. of Copies</u>	<u>Organization</u>
5	National Bureau of Standards Connecticut Avenue & Van Ness St. Washington 25, D. C. Attn: Mr. R. H. Heald	1	Arthur D. Little, Inc. 30 Memorial Drive Cambridge 42, Massachusetts
3	Commanding General Picatinny Arsenal Dover, New Jersey	1	Armour Research Foundation 35 West 33rd Street Chicago 16, Illinois
1	Commanding Officer Diamond Ordnance Fuze Labs. Connecticut Ave. & Van Ness St. Washington 25, D. C.	1	Budd Manufacturing Company Philadelphia, Pennsylvania Attn: Mr. C. L. Eksergian
1	Commanding Officer Watertown Arsenal Watertown, Massachusetts Attn: Dr. R. Beeuwkes, Jr.	1	Baldwin-Lima-Hamilton Corp. Philadelphia 42, Pennsylvania Attn: Strain-Gage Dept.
2	Commanding Officer Chemical Corps Chemical & Radiological Labs. Army Chemical Center, Maryland	1	Case Institute of Technology Cleveland, Ohio Attn: Dr. R. E. Bolts
1	Commanding Officer Watervliet Arsenal Watervliet, New York	1	Franklin Institute 20th Street & Franklin Parkway Philadelphia, Pennsylvania
1	Commanding Officer Rock Island Arsenal Rock Island, Illinois	1	General Electric Company Schenectady, New York Attn: Mr. H. Norris
2	Commanding General Redstone Arsenal Huntsville, Alabama Attn: Dr. Smith	1	Purdue University Aeronautics Department Lafayette, Indiana Attn: Dr. Milton Clauser
1	Commanding Officer Frankford Arsenal Philadelphia 37, Pennsylvania	1	Varian Associates 611 Hansen Way Palo Alto, California Attn: Dr. M. E. Packard
2	Applied Physics Laboratory 8621 Georgia Avenue Silver Spring, Maryland	1	Professor Albert A. Bennett Department of Mathematics Brown University Providence 12, Rhode Island

# DISTRIBUTION LIST

<u>No. of Copies</u>	<u>Organization</u>
1	Professor F. H. Clauser Department of Aeronautics Johns Hopkins University Baltimore 18, Maryland
1	Dr. H. L. Dryden National Advisory Committee for Aeronautics 1724 F. Street, N. W. Washington 25, D. C.
1	University of Virginia Department of Mathematics Charlottesville, Virginia Attn: Prof. Edward J. McShane
1	Dr. L. H. Thomas Watson Scientific Computing Lab. 612 West 116th Street New York 27, New York